Sea Ice Rheology

Daniel L. Feltham

Centre for Polar Observation and Modelling, Department of Earth Sciences, University College London, London WC1E 6BT, United Kingdom, and British Antarctic Survey, Cambridge CB3 0ET, United Kingdom;
email: Daniel.Feltham@cpom.ucl.ac.uk

Annu. Rev. Fluid Mech. 2008. 40:91–112

The *Annual Review of Fluid Mechanics* is online at fluid.annualreviews.org

This article's doi:
10.1146/annurev.fluid.40.111406.102151

0066-4189/08/0115-0091$20.00

Key Words

Arctic, Antarctic, climate model

Abstract

The polar oceans of Earth are covered by sea ice. On timescales much greater than a day, the motion and deformation of the sea ice cover (i.e., its dynamics) are primarily determined by atmospheric and oceanic tractions on its upper and lower surfaces and by internal ice forces that arise within the ice cover owing to its deformation. This review discusses the relationship between the internal ice forces and the deformation of the ice cover, focusing on representations suitable for inclusion within global climate models. I first draw attention to theories that treat the sea ice cover as an isotropic continuum and then to the recent development of anisotropic models that deal with the presence of oriented weaknesses in the ice cover, known as leads.

1. SEA ICE AS A COMPONENT OF THE CLIMATE SYSTEM

Sea ice: frozen sea water that typically consists of floes separated by cracks and leads

Floe: an irregularly shaped sheet of sea ice

Pressure ridge: forms when floes collide and override each other; consists of a sail and keel

Lead: a long, narrow region of open water or thin ice in the sea ice cover

Linear kinematic feature: a long, narrow region of concentrated sea ice deformation observed in satellite-derived imagery (longer than a lead)

As the winter night descends on the polar oceans, the surface mixed layer cools and begins to freeze, forming a floating layer of sea ice. The sea ice covers of the Arctic and Southern Oceans alternately wax and wane seasonally, with sea ice at its maximum extent covering approximately 10% of Earth's oceans.

Much of the sea ice cover is formed from brittle floes that are of approximately convex polygonal shape, have lateral dimensions between 100 m and 5 km, and are typically several meters thick. During winter, the floes weld together to form larger floe aggregates that form a continuous cover (see **Figure 1**). Under imposed stress, exerted by the wind and ocean, sea ice fails to form a network of cracks, typically initiated at existing weaknesses, with a density of approximately 1 km of crack length in every square kilometer of (horizontal) area (Hibler 2001). The floes, or floe aggregates, defined by these cracks, are sensibly rigid and grind along their common edges as they slide past each other in granular motion. Under sufficient compressive stresses, the ice can break up and override to form long, sinuous piles of rubble above and beneath the ice cover, known as pressure ridges (see **Figure 2**). Adjacent cracks may join up to form longer, narrow features, known as leads, whose length typically spans many floe widths (see **Figure 3**). Although the open water in a lead quickly freezes over in winter, a lead typically contains ice thinner than the surrounding floes and is a local weakness in the ice cover. In winter, leads typically occupy approximately 5% of the ice cover. Processing of sequential satellite synthetic aperture radar imagery (Kwok 2001) indicates the presence of concentrated regions of shear in the sea ice cover, known as linear kinematic features, that are several hundred kilometers in length and may be reasonably interpreted as regions of strong lead alignment.

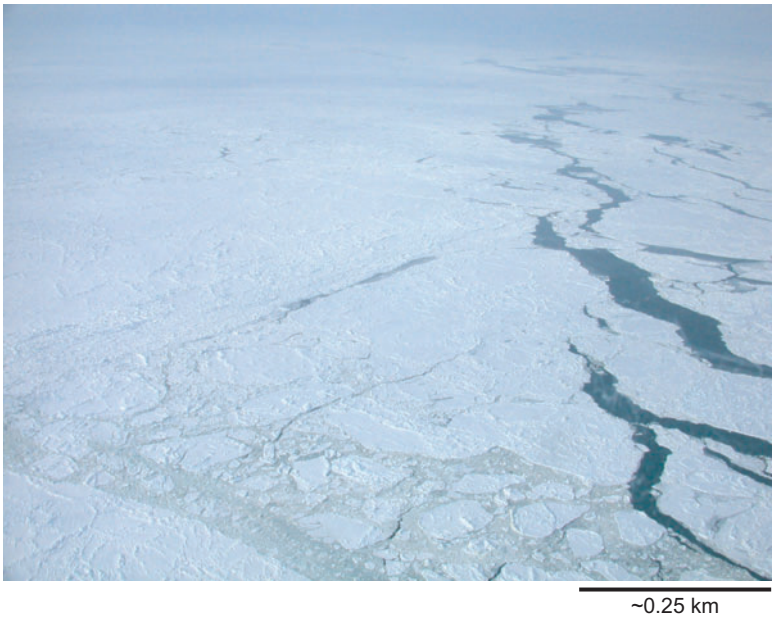

Figure 1

Photograph of a typical region of Arctic sea ice in the east-central Chukchi Sea northwest of Alaska in May 2002, taken from a helicopter. The width of the scene in the foreground is approximately 1 km. Figure reproduced with kind permission from H. Eicken.

Figure 2

Photograph of a pressure ridge in the east-central Chukchi Sea northwest of Alaska in June 2002, taken from an icebreaker. The ridge is fairly narrow, approximately 3 m wide, and formed from ice less than 1 m thick. There is some flooding visible to the right of the ridge owing to the local submergence of the parent ice sheet. The width of the scene in the foreground is approximately 10 m. Figure reproduced with kind permission from H. Eicken.

Sea ice plays an important role in determining polar climate and is believed to influence the global climate in many ways. In particular, (*a*) the high albedo (reflectance) of sea ice and snow-covered sea ice compared with seawater causes reduced solar energy input into the ocean in sea ice–covered regions and a reduction in air temperature over ice-covered seas. The reduction in air temperature can promote further ice formation, leading to the so-called positive albedo feedback mechanism; (*b*) the ice cover reduces the rates of heat and moisture transport between the ocean and atmosphere; (*c*) sea ice provides a dynamic interface that moderates momentum transport between the ocean and atmosphere; and (*d*) as seawater freezes to form sea ice, high salinity brine is expelled (sea ice is approximately 4–10 times less saline than seawater), and as sea ice melts, relatively fresh water is released, both of which affect the thermohaline forcing of the ocean and influence convective overturning and deep-water formation. For these reasons, all modern global climate models contain relatively sophisticated descriptions of the sea ice cover.

The motion and deformation of the sea ice cover, known as its dynamics, are determined by its inertia, atmospheric and oceanic tractions on its upper and lower surfaces, the Coriolis force, sea-surface tilt, and internal ice forces that arise within the ice cover owing to its deformation (discussed below). In this review, I focus on the relationship between the sea ice stress tensor (related to the internal ice force) and

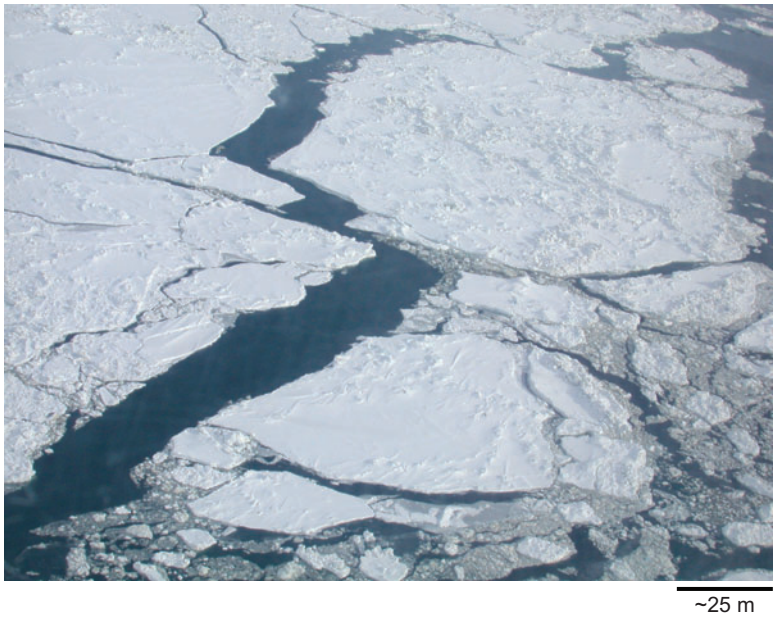

Figure 3

Photograph of a lead in the east-central Chukchi Sea northwest of Alaska in May 2002, taken from a helicopter. The width of the scene in the foreground is approximately 200 m. Figure reproduced with kind permission from H. Eicken.

sea ice deformation, hereafter referred to as sea ice rheology. The included material comprises what I feel are the main theoretical achievements in the development of continuum models of sea ice rheology suitable for inclusion within regional or global climate models. Owing to space limitations, I omit significant studies not directly aligned with this development, such as discrete models (e.g., Hopkins & Tuhkuri 1999, Hopkins et al. 2004) or models of the sea ice edge (e.g., Feltham 2005, Shen et al. 1987). The article is structured as follows: Section 2 describes the momentum balance of sea ice; Section 3 introduces elastic-plastic and viscous-plastic models of sea ice rheology; Section 4 focuses on the principal approaches taken to determine the plastic yield curve; Section 5 draws attention to models of anisotropy of the sea ice cover; and, finally, Section 6 presents some concluding remarks. I have placed much interesting material in Supplementary Appendices, which are available online (follow the Supplemental Material link from the Annual Reviews home page at **http://www.annualreviews.org**); I suggest the interested reader obtain this supplemental information for a more balanced review.

2. MOMENTUM BALANCE OF SEA ICE

Gudkovich & Nikiforov (1963) considered the drift of an individual floe, based on the earlier observations of Nansen (1902), and deduced that the speed and direction of drift depended on floe size and shape. More generally, however, it is necessary to account for interactions between sea ice floes as the floes are either in direct contact, frozen together to form aggregates, or close to each other, possibly separated by refrozen leads.

The Arctic Ice Dynamics Joint Experiment (AIDJEX), a joint venture funded by the United States and Canada, was instigated to study the dynamics of sea ice and its interactions with the atmosphere and ocean. Between 1970 and 1978, AIDJEX scientists made coordinated measurements of atmospheric motion, wind stress, ice strain, ice stress, water motion, and water stress and developed new models and ideas.

Coon et al. (1974) introduced the AIDJEX sea ice model, which considered the ice cover to move in a two-dimensional, horizontal plane. When working with scales much larger than individual floes, one considers the velocity of the sea ice to be defined by a continuously differentiable velocity field $\mathbf{u}(\mathbf{x})$, where $\mathbf{x}$ is the horizontal position in the surface. The deformation rate of the sea ice cover is given by the strain rate

$$\dot{\varepsilon}_{ij} \equiv \frac{1}{2}\left(\frac{\partial u_i}{\partial x_j} + \frac{\partial u_j}{\partial x_i}\right), \tag{1}$$

with principal values $\dot{\varepsilon}_1$ and $\dot{\varepsilon}_2 < \dot{\varepsilon}_1$. It is useful to consider the two invariants given by

$$\dot{\varepsilon}_I \equiv \dot{\varepsilon}_1 + \dot{\varepsilon}_2 = \text{divergence}; \quad \dot{\varepsilon}_{II} \equiv \dot{\varepsilon}_1 - \dot{\varepsilon}_2 = \text{maximum shear rate}, \tag{2}$$

which may also be expressed as

$$\dot{\varepsilon}_I = ||\dot{\boldsymbol{\varepsilon}}|| \cos\theta, \quad \dot{\varepsilon}_{II} = ||\dot{\boldsymbol{\varepsilon}}|| \sin\theta, \tag{3}$$

where

$$||\dot{\boldsymbol{\varepsilon}}|| = \sqrt{\dot{\varepsilon}_I^2 + \dot{\varepsilon}_{II}^2}, \quad \theta = \tan^{-1}\left(\frac{\dot{\varepsilon}_{II}}{\dot{\varepsilon}_I}\right) \tag{4}$$

define the magnitude of the strain rate and the ratio of rates of shearing and divergence, respectively. In particular, $\theta = 0, \pi/4, \pi/2, 3\pi/4$, and π correspond to pure divergence, uniaxial extension, pure shear, uniaxial contraction, and pure convergence, respectively.

The AIDJEX (horizontal) momentum balance for sea ice was deduced through a consideration of the forces acting on a single floe with an additional force due to interactions between floes:

$$\frac{D(m\mathbf{u})}{Dt} = -mf_C\mathbf{k} \times \mathbf{u} + \boldsymbol{\tau}_a + \boldsymbol{\tau}_w - m\hat{g}\Delta H + \nabla \cdot \boldsymbol{\sigma}, \tag{5}$$

where each term has units of force per unit area of the sea ice cover, and t is time. The rate of change of momentum (left-hand side of Equation 5) is set equal to the balance of forces (the right-hand side), which are as follows (from left to right): Coriolis force, atmospheric drag, ocean drag, force due to sea-surface tilt, and the ice interaction force given by the divergence of the sea ice stress tensor. The sea ice stress tensor σ_{ij} is the integral of the Cauchy stress tensor through the depth of the sea ice, in excess of the isostatic stress $\frac{1}{2}\rho_{\text{ice}}h^2\hat{g}\delta_{ij}$ (where ρ_{ice} is the ice density, $\hat{g}$ is the acceleration due to gravity, and h is the ice depth). In the momentum equation, D/Dt is the material derivative, $\mathbf{k}$ is the unit vector normal to the ice surface directed into the atmosphere, f_C is the Coriolis parameter, m is the ice mass per unit area, and H is the sea-surface dynamic height. The ice mass is determined by

$$m = \rho_{\text{ice}} \int_0^\infty g(h)h\,dh, \tag{6}$$

where $g(h)$ is the thickness distribution function defined such that the fractional area of ice with thickness in the range h to $h + dh$ is given by $g(h)dh$. Force-balance calculations using reasonable parameterizations for air and ocean drags and sea ice stress (Steele et al. 1997) show that the acceleration term is negligible for timescales much larger than a day, and the sum of the Coriolis and sea-surface tilt terms is always small compared with the remaining terms. On timescales greater than weeks, the force balance is typically dominated by atmospheric drag, oceanic drag, and the ice interaction force with the precise balance depending on time and location.

The evolution of the ice thickness distribution is given by

$$\frac{Dg}{Dt} = \Psi - g\left(\dot{\varepsilon}_I + \frac{\partial f}{\partial h}\right), \tag{7}$$

where Ψ is the redistribution function, and f is the vertical freeze/melt rate (Thorndike et al. 1975). The redistribution function Ψ accounts for the mechanical redistribution of thin ice into ridges of thicker ice during convergence and for the production of open water as a result of divergence; it may be expressed as

$$\Psi = ||\dot{\varepsilon}||[\alpha_r(\theta)\psi + \chi(h)\alpha_o(\theta)], \tag{8}$$

where $\alpha_r(\theta)$ and $\alpha_o(\theta)$, known as the ridging and opening coefficients, describe the relative amount of deformation realized through pure convergence–type ridging and pure divergence–type opening, respectively [defined such that $\alpha_r(\pi) = 1$, $\alpha_o(0) = 1$, and $\alpha_0 = \alpha_r + \cos\theta$]. The function $\chi(h)$ is twice the Dirac delta function, so defined that $\chi(h) = 0, \forall h > 0$ and $\int_0^\infty \chi(h)dh = 1$.

Gray & Morland (1994) subsequently derived the horizontal momentum balance for sea ice more systematically from the three-dimensional momentum and mass balance equations for the sea ice and ocean using mixture (interacting continua) theory. These equations were simplified by integration through layer depth and by exploiting the small geometrical aspect ratio of an individual floe and the smallness of the ratio of the magnitude of horizontal to vertical (gravitational) forces. To leading order, this determined a two-dimensional momentum balance of similar form to Equation 5. However, the momentum balance determined by Gray & Morland applies to the mixture of sea ice and the water between the floes because otherwise the unknown ice–ocean actions must be taken into account (these cancel out when the momentum balance of the ice is added to that of the water).

3. SEA ICE RHEOLOGY

The relationship between sea ice stress $\boldsymbol{\sigma}$, caused by floe–floe or floe–lead interactions, to the large-scale deformation of the ice cover $\dot{\boldsymbol{\varepsilon}}$, the material properties of sea ice, and the state of the ice cover is known as sea ice rheology. The determination of suitable constitutive relations to describe sea ice rheology has guided sea ice–dynamics research since it began, and it remains an outstanding problem that limits the success of sea ice models.

Early models of sea ice rheology, such as those of Ruzin (1959) and Reed & Campbell (1960), parameterized the stress resulting from interactions between sea

ice floes using a two-dimensional Laplacian operator with an effective, constant eddy viscosity, i.e., effectively treating the ice cover like a viscous fluid. However, observations of flow with weak horizontal divergence led Rothrock (1970) and Solomon (1970) to include a pressure term to prevent unrealistic convergence in the Beaufort Sea. Subsequent theoretical development of models of sea ice rheology was revolutionized through the conception of sea ice as a plastic material, as introduced in the AIDJEX model.

3.1. Elastic-Plastic Sea Ice Rheology

The AIDJEX sea ice model treats the macroscopic mechanical behavior of sea ice using an elastic-plastic rheology. **Supplemental Appendix A** gives a brief description of plasticity (follow the Supplemental Material link from the Annual Reviews home page at **http://www.annualreviews.org**). The strongest argument for adopting a plastic model for sea ice is that, despite relatively smooth variations in atmospheric and oceanic forcing fields, local events such as ridging and formation of leads occur sporadically and irreversibly, as though a critical stress state in the ice had been reached. In addition, theoretical arguments suggest that, provided the shape of a pressure ridge is independent of the rate at which it forms, the nonrecoverable work done against gravity (Parmerter & Coon 1973, Rothrock 1975) and sliding friction (Rothrock 1975) is also rate independent. A final argument for plastic behavior invokes a compelling visual analogy between sea ice and such granular materials as soils, which have been modeled successfully as a plastic (Schofield & Wroth 1968).

The case for an elastic (subcritical) response was largely made for mathematical convenience: A rigid plastic model does not allow subcritical stresses to be calculated, so it is not possible to decide if the stress is critical or subcritical, i.e., whether there is plastic deformation or no deformation. In addition, Coon et al. (1974) reasoned that, in a dense pack, thick floes are wedged together with little thin ice present, so as subyield stresses are applied, there can be only elastic deformations in the thick floes. The deformations are negligible compared with plastic deformations associated with opening and closing cracks, but the elastic stresses can be large and must be evaluated.

Coon et al. (1974), and most subsequent modelers, considered sea ice to be isotropic, which allows the plastic yield surface to be expressed as a yield curve in the plane of the principal stresses σ_1 and σ_2 or, equivalently, through the stress invariants σ_I and σ_{II}, where

$$\sigma_I \equiv \frac{1}{2}(\sigma_1 + \sigma_2) = \text{negative pressure}; \quad \sigma_{II} \equiv \frac{1}{2}(-\sigma_1 + \sigma_2) = \text{maximum shear stress}. \tag{9}$$

The yield criterion is written as

$$F(\sigma_I, \sigma_{II}; \text{scalars}) = 0, \tag{10}$$

where F is the (scalar) yield function and defines a family of yield curves in the $\{\sigma_I, \sigma_{II}\}$ plane owing to the variation of the scalar properties of the sea ice. For an isotropic material, F must be symmetric about $\sigma_{II} = 0$ (Truesdell & Noll 1965).

The strain rate is typically split into elastic $\dot{\varepsilon}^e$ and plastic $\dot{\varepsilon}^p$ components, where, by assumption, $\dot{\varepsilon} = \dot{\varepsilon}^e + \dot{\varepsilon}^p$. The elastic strain is related to stress through an elastic law, and the plastic strain rate is related to stress through a plastic flow law and is zero when the stress state lies within the yield curve. Strain must be measured relative to an unloaded (stress-free) reference configuration, which is constantly evolving owing to plastic deformation (Pritchard 1975).

Whenever the stress state lies on the yield curve, irreversible plastic deformation occurs. Coon et al. (1974) adopted the associated normal flow law

$$\dot{\varepsilon}_k^p = \lambda \left. \frac{\partial F}{\partial \sigma_k} \right|_{F=0} \quad k = I, II, \tag{11}$$

where $\dot{\varepsilon}_k^p$ is the plastic strain rate, and λ is an unknown, positive scalar that is determined as part of the solution of the dynamical equations. Equation 11 states that at a given stress state on the yield curve, the plastic strain rate is in the direction of the exterior normal to the yield curve but is of unknown magnitude; i.e., the normal flow rule specifies the ratio of shear straining to divergence for each point on the yield curve but places no restriction on their absolute rates. Almost all models of sea ice dynamics use this flow rule; its justification largely seems based on its successful application to granular materials such as soils and its satisfactory performance (within the limits of experimental error and parameter tuning) in sea ice simulations.

3.2. Viscous-Plastic Sea Ice Rheology

Hibler (1979) based his sea ice model on the isotropic, plastic approach of Coon et al. (1974) but replaced the elastic-subplastic yield behavior with a viscous behavior. Hibler introduced this rheology in part to avoid the need to keep track of an evolving unload configuration from which to measure strain. To reduce the computational burden of calculating the evolution of a thickness distribution, Hibler also replaced the thickness distribution with just two categories: (*a*) thick ice of thickness h and area fraction (concentration) A and (*b*) thin ice (which included open water) with area concentration $1 - A$. Evolution equations were introduced for the thick-ice thickness and area concentration, which included artificial (regularizing) diffusion terms.

The concept of a viscous subyield behavior came from the idea that the random jostling of a collection of perfectly plastic floes leads to an averaged viscous behavior of the collection of floes at small averaged strain rates. Hibler (1977) showed that when a two-dimensional, rigid plastic model with an elliptical yield curve is used, large stochastic variations in strain rate compared with the mean strain rate cause the relationship between averaged stress and averaged strain rate to be approximately linear viscous with a pressure term.

An essential difference between the viscous-plastic rheology and the elastic-plastic rheology is the way in which relatively motionless ice is treated: In the elastic-plastic case, a high stress can be maintained without any relative motion, whereas in the viscous-plastic case, such stationary states are approximated by a state of very slow flow or creep. By using sufficiently large viscosities, one can make the strain rate

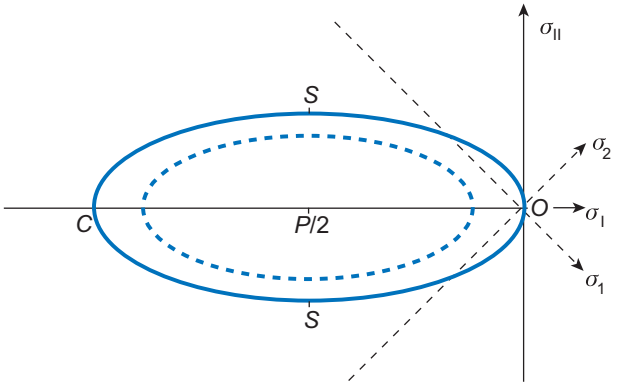

Figure 4

Elliptical yield curve for a viscous-plastic rheology. For plastic flow, the stress state lies on the solid curve with the location determined by the ratio of strain rate principal components; e.g., the stress state for pure shear is located at *S*, pure convergence is at *C*, and pure divergence is at *O*. For very small strain rates, the stress state moves inside the yield curve as illustrated by the dashed ellipse.

at which plastic behavior occurs effectively negligible, and the viscous-plastic model does not make a distinction between the plastic strain rate and the total strain rate.

The plastic and viscous behavior can be represented using the standard (reduced) Reiner-Rivlin form (e.g., Hunter 1983),

$$\sigma_{ij} = 2\eta\dot{\varepsilon}_{ij} + [\zeta - \eta]\dot{\varepsilon}_{kk}\delta_{ij} - P\delta_{ij}/2, \tag{12}$$

where $P/2$ is a pressure term. Hibler (1979) chose $\zeta(\dot{\varepsilon}_{ij}; P)$ and $\eta(\dot{\varepsilon}_{ij}; P)$ to depend on $\dot{\varepsilon}_{ij}$ and P in such a way as to ensure that for typical strain rate magnitudes, the normal plastic flow law applies and the stress state lies on an elliptical yield curve passing through the origin (so there is no ice stress for pure divergence) (see **Figure 4**). The general shape of the yield curve was chosen to agree with the expected behavior of sea ice (namely that it should be weak in tension, strong in shear, and strongest in compression) and to satisfy the requirements of continuum mechanics (namely that it should not be concave and should be symmetric about the σ_I axis). The particular choice of an elliptical yield curve, however, was solely made for mathematical convenience because this allowed ζ and η to be expressed in closed form:

$$\zeta = P/2\Delta, \quad \eta = \zeta/e^2, \tag{13}$$

where

$$\Delta = \left[\left(\dot{\varepsilon}_{11}^2 + \dot{\varepsilon}_{22}^2\right)\left(1 + e^{-2}\right) + 4e^{-2}\dot{\varepsilon}_{12}^2 + 2\dot{\varepsilon}_{11}\dot{\varepsilon}_{22}\left(1 - e^{-2}\right)\right]^{1/2}, \tag{14}$$

and e is the yield curve eccentricity. Hibler defined upper bounds on ζ and η, dependent on the ice strength P, which are reached at small strain rates (creep) and cause the stress state to lie on a concentric ellipse inside the yield curve, as in **Figure 4**. In practice, these upper values are chosen to be large enough that they do not significantly affect the calculations of ice motion.

The viscous-plastic rheology is completed with an equation of state for the ice strength, or pressure. Hibler (1979) used

$$P = P^* h \exp[-C(1 - A)], \tag{15}$$

where P^* and C are fixed (positive) empirical constants. For high concentrations of thick ice A, more thick ice is deformed, and the strength depends on the thick-ice thickness h. For a large amount of thin ice, $1 - A$ approaches unity, and the effective ice strength decreases significantly. Although it predicts feasible trends of ice strength, there is dubious justification for the precise form of the strength equation, with the constant P^* in particular being frequently tuned within a factor of 10 or so of about 10^5 Nm^{-1} to improve correspondence with observations (C is normally fixed at $C = 20$).

Hibler's viscous-plastic rheology, or, more recently, a numerically efficient variant that includes some artificial elasticity to render the stress calculation explicit (often misleadingly referred to as the elastic-viscous-plastic rheology) (Hunke & Dukowicz 1997), has been implemented in many sea ice and climate models. **Supplemental Appendix B** discusses some undesirable features of the Hibler (1979) sea ice model and its subsequent modification.

4. DETERMINATION OF THE PLASTIC YIELD CURVE

A model framework in which the sea ice cover is treated as an isotropic continuum that routinely deforms plastically has dominated approaches to modeling sea ice rheology since the AIDJEX model was first introduced. Subsequent effort has largely focused on determining an appropriate plastic behavior. Two main approaches have been taken: (*a*) determination of the plastic yield curve and flow rule through a consideration of the energetics of subcontinuum-scale deformation of the ice cover and (*b*) imposition of a scale-invariant, Mohr-Coulomb rheology.

4.1. Energetics of Subcontinuum Deformation

Rothrock (1975) generalized the earlier arguments of Parmerter & Coon (1973) to develop a relationship between the plastic yield curve shape and size and the redistribution of ice thickness during the formation of a pressure ridge. He did this by equating the plastic work of deformation to the gravitational potential energy of a pressure ridge and frictional losses in the formation of the ridge. Two sinks of energy were knowingly neglected: the loss of energy due to fracture of the ice sheet, which was shown by Parmerter & Coon to be negligible, and the frictional loss in shearing between floes. The frictional loss due to shearing was later shown to be significant (Pritchard 1981, Ukita & Mortiz 1995, Wilchinsky et al. 2006), but this does not qualitatively affect Rothrock's arguments.

Rothrock assumed an isotropic constitutive equation with the alignment of the principal axes of stress and strain rate and, as his central hypothesis, set

$$\sigma_I \dot{\varepsilon}_I + \sigma_{II} \dot{\varepsilon}_{II} = R_{\mathrm{pot}} + R_{\mathrm{fric}}. \tag{16}$$

The left-hand side of this equation is the rate of doing plastic work per unit area, R_{pot} is the rate of the mechanical production of gravitational potential energy per unit area, and R_{fric} is the rate of frictional energy dissipation per unit area. After calculations, Rothrock showed that the rate of doing plastic work is

$$\sigma_I \dot{\varepsilon}_I + \sigma_{II} \dot{\varepsilon}_{II} = ||\dot{\varepsilon}|| \alpha_r(\theta) P^*, \tag{17}$$

where the right-hand side contains both the rate of potential energy production and the frictional energy loss combined into the factor P^*,

$$P^* = \xi \int_0^\infty h^2 a(h) dh, \tag{18}$$

where $a(h)$ is the distribution of thin ice lost in ridging, and ξ is a constant related to the density difference between ice and seawater, the coefficient of friction of ice, the ridge angle of repose, and the thickness redistribution in ridging. The parameter P^* is the strength of the ice pack in pure convergence. To see this, let us consider the case $\dot{\varepsilon}_I = -||\dot{\varepsilon}||$, $\dot{\varepsilon}_{II} = 0$, and $\alpha_r(\pi) = 1$ for which Equation 17 states that convergence can only occur if the compressive stress σ_I is equal to $-P^*$. Weaker stresses cannot do enough work to build ridges and therefore do not cause deformation.

Using Equation 3 and nondimensionalizing stress with P^*, we can rewrite the plastic power (Equation 17) as

$$\sigma_{II} = -\frac{1}{\tan\theta}\sigma_I + \frac{\alpha_r(\theta)}{\sin\theta}. \tag{19}$$

Rothrock (1975) assumed that the normal plastic flow law applies; simple geometry gives the angle between the σ_I axis and the yield curve's normal as

$$\tan\theta = -\left(\frac{d\sigma_{II}}{d\sigma_I}\right)^{-1}. \tag{20}$$

Equations 19 and 20 constitute a nonlinear differential equation for $\sigma_{II}(\sigma_I)$ and allow the calculation of the plastic yield curve. Although Rothrock demonstrated a relationship between the ridging coefficient $\alpha_r(\theta)$ and the plastic yield curve $\sigma_{II}(\sigma_I)$, there was no rationale given for determining either one independently, except that the yield curve should be physically reasonable.

Ukita & Moritz (1995, 2000; Moritz & Ukita 2000) generalized Rothrock's approach by including an energy sink due to the sliding motion of floes parallel to cracks in Equation 17 and by providing a method of determining the ridging and sliding coefficients. Ukita & Moritz's rate of plastic work equation (divided by the strain rate magnitude, $||\dot{\varepsilon}||$) is

$$\sigma_I \cos\theta + \sigma_{II} \sin\theta \cos 2\gamma = P^*[\alpha_r(\theta) + k\alpha_s(\theta)], \tag{21}$$

where the sliding coefficient $\alpha_s(\theta)$ has been introduced, the parameter k is the ratio of energy transformations associated with sliding relative to ridging, and γ is the angle between the directions of principal stress and strain rate (which were not initially assumed to be parallel). Ukita & Moritz simplified their analysis by setting $P^* = 1$ and only considering $\sigma_I \leq 0$. They used a principle of minimization of maximum

shear stress σ_{II} as σ_I, γ, and θ varied that led to $\gamma = 0$ and expressions for the yield curve and flow rule.

Moritz & Ukita (2000) determined the ridging and sliding coefficients, $\alpha_r(\theta)$ and $\alpha_s(\theta)$, respectively, using a kinematic model: (*a*) They divided a plane region into an irregular, random tiling of convex polygon floes separated by cracks (leads), obtained using the Poisson process (see Moritz & Ukita 2000 for details); (*b*) they used a Taylor expansion of the continuum velocity field to find the rigid body velocity of each of the floes, assuming no spinning of the floes, and used the difference between adjacent floe velocities to calculate the rate of opening/closing and sliding in the cracks separating the floes; and, finally, (*c*) they summed the rates of opening/closing and sliding from all the cracks to determine the opening coefficient $\alpha_o(\theta)$, ridging coefficient $\alpha_r(\theta)$, and sliding coefficient $\alpha_s(\theta)$.

Figure 5 shows the yield curves obtained by minimizing σ_{II} using $\alpha_r(\theta)$ and $\alpha_s(\theta)$ calculated for the randomly determined convex polygons. With $k = 0$ (no frictional energy of sliding), the yield curve has a sine-lens shape. With sliding, there is an increase in the maximum shear stress, as well as an elongation along the σ_I axis. With sliding, there is asymmetry between the divergent ($d\sigma_{II}/d\sigma_I < 0$) and convergent ($d\sigma_{II}/d\sigma_I > 0$) regimes, resulting in a teardrop shape. This can be understood by realizing that for the same ratio of the magnitude of shearing to divergence, closing and sliding at cracks result in larger shear stresses than opening and sliding at cracks. Similar reasoning led Rothrock (1975) and Coon et al. (1974) to suggest teardrop shapes for the yield curve.

Although Ukita & Moritz (1995) included the role of frictional sliding into the plastic deformation power equation, by normalizing the rate of work done with a constant ice strength (setting $P^* = 1$), they ignored the different dependence of ridging

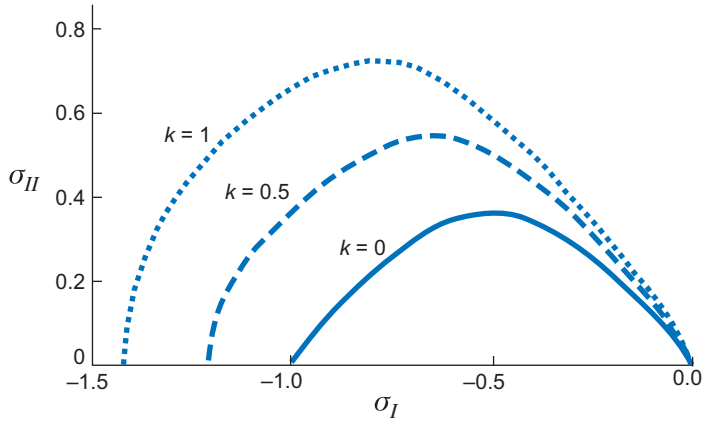

Figure 5

Yield curves computed by minimizing shear stress using ridging and sliding coefficients calculated using a random isotropic geometry with varying values of frictional energy loss k. Without the contribution from sliding ($k = 0$), the yield curve has a sine-lens shape. As k increases, the yield curve shape changes to tear dropped and becomes more asymmetric. Figure adapted from Ukita & Moritz 2000.

work and sliding work on ice thickness. Wilchinsky & Feltham (2004b) addressed this deficiency for an ice cover of uniform thickness (which was considered in Ukita & Moritz's theory), and Wilchinsky et al. (2006) generalized this to an ice cover with a discrete thickness distribution. Because the ridging and sliding coefficients, α_r and α_s, determined by Moritz & Ukita (2000) were found from kinematic considerations concerning floe geometry but not ice thickness, Wilchinsky et al. adopted the same ridging and sliding coefficients for an ice cover consisting of ice of various thicknesses. They wrote the rate of doing plastic work of a nonuniform-thickness sea ice cover (divided by the strain rate magnitude, $||\dot{\varepsilon}||$) as

$$\sigma_I \cos\theta + \sigma_{II} \sin\theta = P_r \alpha_r(\theta) + P_s \alpha_s(\theta) + P_o \alpha_o(\theta), \tag{22}$$

where the final term accounts for work done in opening, and they demonstrated that the ridging, sliding, and opening contributions can be considered separately,

$$\boldsymbol{\sigma}(\dot{\varepsilon}) = P_r \boldsymbol{\sigma}^r(\dot{\varepsilon}) + P_s \boldsymbol{\sigma}^s(\dot{\varepsilon}) + P_o \boldsymbol{\sigma}^o(\dot{\varepsilon}), \tag{23}$$

where P_r, P_s, and P_o are the ridging, sliding, and opening strengths, respectively, and $\boldsymbol{\sigma}^r(\dot{\varepsilon})$, $\boldsymbol{\sigma}^s(\dot{\varepsilon})$, and $\boldsymbol{\sigma}^o(\dot{\varepsilon})$ are the normalized (i.e., independent of ice thickness h) ridging, sliding, and opening stress tensors, respectively, determined by the pairs of coupled equations

$$\left.\begin{aligned} \sigma_I^x \cos\theta + \sigma_{II}^x \sin\theta &= \alpha_x(\theta) \\ \sigma_{II}^x &= \min_\theta \left(\tfrac{\alpha_x(\theta)}{\sin\theta} - \sigma_I^x \cot\theta \right) \end{aligned}\right\} (x = r, s, o). \tag{24}$$

The solutions $\{\sigma_I^r(\theta), \sigma_{II}^r(\sigma_I^r)\}$, $\{\sigma_I^s(\theta), \sigma_{II}^s(\sigma_I^s)\}$ were calculated numerically using the ridging and sliding coefficients of Moritz & Ukita (2000) [the normalized opening stress $\boldsymbol{\sigma}^o(\dot{\varepsilon})$ can be linearly related to the ridging stress $\boldsymbol{\sigma}^r(\dot{\varepsilon})$]. The direction of the strain rate for each of the ridging, sliding, and opening yield curves was found to be nearly normal to the yield curves.

The sea ice stress (Equation 23) depends on the thickness distribution through the ridging P_r, sliding P_s, and opening strengths P_o. The ridging ice strength was determined using results from the discrete element simulation of ridge formation by Hopkins (1998); the sliding ice strength was determined by assuming a linear friction law acts as floes slide past each other; and the opening strength was set to zero because the limited data available suggest it is very small. As the thickness distribution varies, the relative contribution of ridging, sliding, and opening to the total sea ice stress may vary (resulting in a slight change of shape of the yield curve). For example, because thick ice is hard to ridge, the sea ice stress of an ice cover containing relatively thick ice is determined predominantly by frictional sliding and opening. Wilchinsky et al. (2006) included their new sea ice rheology into the sea ice component of a global climate model (Los Alamos CICE model, version 3.0) and showed that their new rheology helped to more accurately model the spatial distribution of ice in the central Arctic Ocean, as compared with submarine observations.

4.2. Mohr-Coulomb Failure

The arguments in the above section relate the continuum-scale plastic behavior to the subcontinuum deformation; another popular approach has been to simply assert a continuum-scale yield curve based on the idea of shear fracture or frictional sliding along flaws. In terms of determining a continuum-scale yield curve, shear fracture and frictional sliding are treated in the same way. The traction on a line in a horizontal plane of sea ice is given by

$$\boldsymbol{\sigma} \cdot \mathbf{n} = \sigma_n \mathbf{n} + \tau_n \mathbf{t}, \tag{25}$$

where $\mathbf{n}$ and $\mathbf{t}$ are the unit normal and tangent vectors to this line, respectively; σ_n is the normal stress across the line; and τ_n is the shear stress along the line. In the application of Mohr's theory to sea ice rheology, failure (i.e., flow) of the ice cover occurs when the component of shear stress τ_n attains a critical value related to the component of normal stress σ_n given by Mohr's failure law:

$$|\tau_n| = \Omega(\sigma_n; \text{scalars}). \tag{26}$$

The sea ice is assumed to be perpetually in a critical state in which the above relation holds along what are known as slip lines. The slip lines are at an angle, measured from the principal directions of stress, that minimizes the shear stress τ_n. One can easily show that the angle between the principal direction σ_1 and the slip line normals is

$$\psi_{\pm} = \pm(\pi/4 - \Theta/2), \tag{27}$$

where the angle of internal friction Θ is defined by

$$\tan\Theta = -\frac{1}{\Omega'}, \tag{28}$$

where Ω' is the total derivative of Ω with respect to its argument. The shear and normal stresses, τ_n and σ_n, are related to the isotropic pressure σ_I and maximum shear stress σ_{II} through

$$\tau_n^2 + (\sigma_n + \sigma_I)^2 = \sigma_{II}^2, \tag{29}$$

which defines the Mohr circle in the $\{\sigma_n, \tau_n\}$ plane. As **Figure 6** shows, the envelope of the set of Mohr circles (obtained as σ_I varies) comprises two yield curves associated with the failure law (Equation 26).

Erlingsson (1988) suggested that, depending on the boundary conditions on the sea ice deformation field, the slip lines were collinear with pressure ridges and orthogonal to leads. Thus observations of ridges and leads, assumed to be at a fixed angle to the slip lines, would allow one to determine the directions of the slip lines, the angle of internal friction, and deduce the stress law. [Pritchard (1988) made a similar suggestion with regard to the characteristics of strain rate in a model with a more general plastic rheology.] Erlingsson (1988) examined several images, including Landsat imagery of the ice field off the Greenland coast (1976) and Seasat SAR images for the central Arctic (1986), and determined $\Theta = 15° \pm 2°$ over horizontal length scales from 100 m to 100 km. He took this to imply that the internal angle of friction was a scale-invariant property that could be used to relate sea ice dynamics over a range of length scales. Although Erlingsson's ideas are promising, they have not been taken much further,

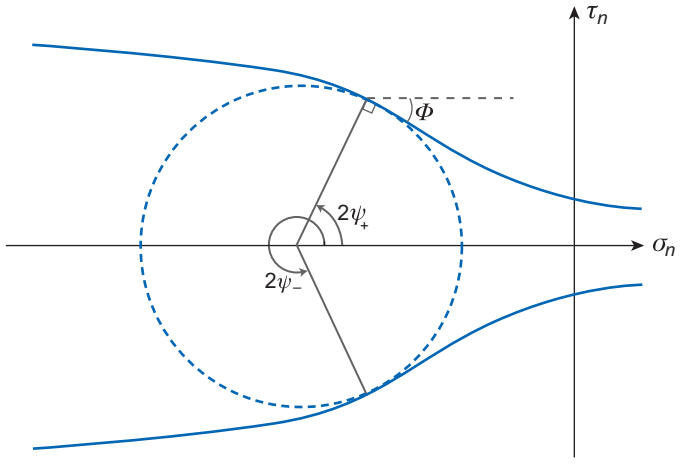

Figure 6

The symmetrical yield criterion $|\tau_n| = \Omega(\sigma_n;\text{scalars})$ and the Mohr circle at the point with internal angle of friction Φ.

which is probably because of the complexity of the observed ice cover, which makes the identification of active leads and ridges (as opposed to fossils of past deformation) difficult.

Tremblay & Mysak (1997) presented a dynamic sea ice model based on a granular material rheology for sea ice (i.e., they did not consider the initial failure of a homogeneous cover). For sea ice deformation along a sliding line, the failure criterion, which Tremblay & Mysak chose to be given by Coulomb's fiction law (a special case of Mohr's failure law), must be met:

$$\tau_n = \sigma_n \tan\Theta + \mathcal{S}, \tag{30}$$

where Θ is now a constant angle of internal friction, and $\mathcal{S}$ is the inherent shear strength (cohesion) and is set to zero. For stress ratios $\tau_n/(-\sigma_n)$ less than $\tan\Theta$, deformation does not occur, and when the stress ratio equals $\tan\Theta$, Tremblay & Mysak asserted that the sea ice deforms by sliding equally along the two sliding lines. Writing the traction components τ_n and σ_n in terms of the stress invariants, one can rewrite the failure criterion (Equation 30) as

$$\sigma_{II} = -\sigma_I \sin\Theta, \tag{31}$$

and Tremblay & Mysak limited the pressure $-\sigma_I$ to a maximum value of P, set equal to Hibler's (1979) ice strength (Equation 15). When $-\sigma_I$ reaches this value, the ice can no longer support the compressive load, the floes override each other, and a pressure ridge forms. **Supplemental Figure 2** shows the yield curve described by these equations in stress-invariant space (follow the Supplemental Material link from the Annual Reviews home page at **http://www.annualreviews.org**). Note that the normal flow rule does not apply here, but the global strain rate can be related to the rate of sliding along the sliding lines under the assumption of no spinning.

Tremblay & Mysak (1997) considered the divergence associated with the shearing of a granular assembly. The angle between the plane of motion of individual grains (floes) and the macroscopic sliding plane is called the angle of dilatancy, denoted

δ. They showed that the angle of dilatancy modified the effective angle of internal friction to

$$\Theta_{\text{eff}} = \Theta + \delta, \tag{32}$$

and, for simplicity, assumed the effective angle of internal friction to have reached a saturation value, which they set to $\Theta_{\text{eff}} = 30°$ based on the observations of Overland & Pease (1988).

5. ANISOTROPY OF THE SEA ICE COVER

Because leads contain ice that is thinner than the thick ice in which they are embedded, they determine the stresses that can be maintained in the ice layer, and because leads are oriented features, this introduces anisotropy at the scale of the leads. The constitutive laws for continuum-scale sea ice stress described above are isotropic. Aside from the huge theoretical convenience of the assumption of isotropy, the most compelling argument cited in its favor is that on length scales of 100 km and greater, the distribution of leads appears to be nearly isotropic (e.g., Coon et al. 1974, Hibler 1979, Rothrock 1975) so that a mean-field rheology is isotropic. However, increasing evidence has shown that lead orientation, at least in the central pack, has a marked bimodality with the leads defining diamond-shaped floe aggregates (e.g., Hibler 2001, Schulson 2004). Coon et al. (1998) argue from field observations and stress measurements that length scales of the order of 100 km and timescales of several weeks are required for a model grid cell to contain three or more active leads. To parameterize dynamic processes at resolutions finer than 100 km (and timescales finer than several weeks), one must consider the effect of one or a few leads on the local rheology. If one believes that the sea ice rheology is truly scale invariant, so that the rheology of the large-scale ice pack is the same as that of an individual floe, then running an existing isotropic rheology sea ice model at sufficiently fine resolution would enable the accounting of the dynamics of leads. **Supplemental Appendix C** presents a discussion of scale-invariant and scale-dependent approaches to sea ice rheology.

The investigation of anisotropic models of sea ice dynamics is relatively recent. By combining the yield curves of floes and one or two leads, Coon et al. (1998) constructed the composite yield surface for a given strain rate. With two leads of weak ice at an angle, for example, the composite yield surface predicts sliding before ridging can occur at all. Hibler & Schulson's (2000) approach has been to apply the continuity of normal traction at the interfaces of thick ice (floes) and thin ice (leads). Explicit calculation of the strain rates for an imposed stress allows the calculation of the variation of preferred flaw (lead) orientation as the confinement ratio of stresses is varied. Schreyer et al. (2006) considered an elastic-decohesion model of sea ice failure that is used to indicate when a lead is initiated, its mode of failure, and the subsequent evolution of the lead (decohesion). **Supplemental Appendix D** discusses these developments in more detail.

The models of anisotropy discussed above consider lead formation and the influence of one or several leads on the local failure stress. However, as these models

require that the orientation and characteristics of each lead are known at all times, calculations of stress and dynamics are impractical on an ocean-basin scale. Wilchinsky & Feltham's (2004a, 2006a,b) approach has been to develop an anisotropic model of sea ice dynamics that is simple enough to be incorporated into climate models. The model consists of a mean-field sea ice rheology that depends on continuous and differentiable tensor variables describing the orientation of leads, and the orientation weighted by lead ice thickness and width, and evolution equations for these variables.

5.1 A MEAN-FIELD ANISOTROPIC SEA ICE MODEL

To construct a tractable continuum anisotropic sea ice model, Wilchinsky & Feltham (2004a) introduced a representative area element (RAE) that is equally subdivided into square basic elements, each of which contains one lead passing through its center (see **Figure 7**). The RAE contains a representative sample of thick ice and disconnected leads and defines the smallest length scale at which it makes sense to apply a continuum approach. In the RAE, the formation or termination of a lead of given orientation, width, and thickness is accounted for by changing the probability of this lead being found in a basic element. Lead length change within a basic element is determined by the deformation of the thick ice so that lead length is not tracked within a basic element. The lengthening of a lead across the RAE is determined by the realignment of the leads in the adjacent basic elements along the lead direction. Because the RAE generally contains disconnected leads in the basic elements, the deformation of these leads is accompanied by the deformation of the thick ice, and their rotation is determined by the global deformation (Hibler 2001, Stern et al. 1995).

Owing to the presence of a lead in a basic element, the local (i.e., basic element) strain rate is not uniform and is generally different from the strain rate $\dot{\epsilon}$ applied to

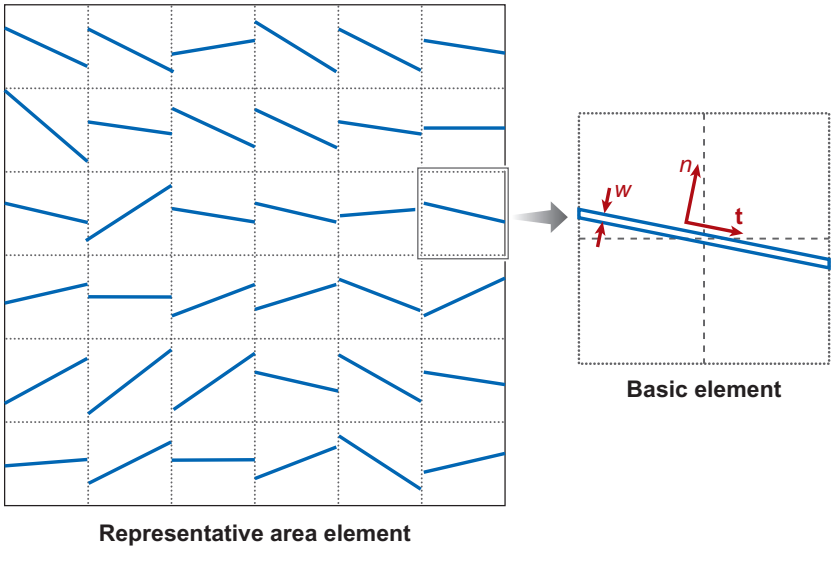

Figure 7

A representative area element of sea ice consisting of square basic elements and single leads completely intersecting them. Figure adapted from Wilchinsky & Feltham 2004a.

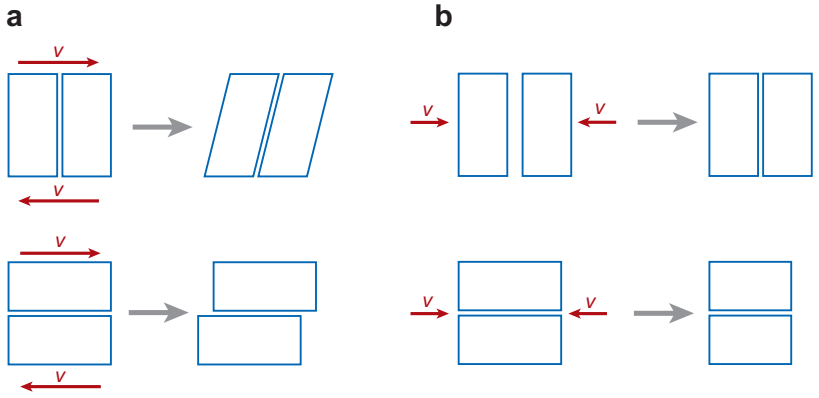

Figure 8

A basic element under a shearing deformation (*a*) and uniaxial compression (*b*) without interaction with the adjacent basic elements. Figure adapted from Wilchinsky & Feltham 2004a.

the RAE (see **Figure 8**). Shearing of a basic element along its lead, and compression across it, occurs through deformation inside the lead only (the lead is active), whereas shearing of the basic element across the lead and compression along it occur mainly through the deformation of the thick ice (the lead is passive). Wilchinsky & Feltham (2004a, 2006a) summed the contributions of lead and thick-ice stress to give a basic element stress, accounted for interactions between adjacent basic elements, and averaged over all possible lead configurations to obtain an expression for the continuum, RAE stress. They made assumptions to reduce the dependency of the RAE sea ice stress to the form

$$\boldsymbol{\sigma} = \boldsymbol{\sigma}(\dot{\varepsilon}, \mathbf{A}, \mathbf{R}), \tag{33}$$

where

$$\mathbf{A} = \langle \mathbf{t} \otimes \mathbf{t} \rangle \quad \text{and} \quad \mathbf{R} = \langle h^{2\alpha} \mathbf{t} \otimes \mathbf{t} \rangle \tag{34}$$

are known as the structure tensor and thickness tensor, respectively, and $\otimes$ denotes the dyadic (tensor) product. The averaging operator $\langle \cdot \rangle = \int_0^H \int_0^1 \int_S (\cdot) \phi d\mathbf{t} dw dh$, where S is a unit-radius circle in R^2, and $\phi(\mathbf{t}, h, w)$ is the probability density function for finding a lead along the direction of unit vector $\mathbf{t}$ and with thickness h and width w in any given basic element [$\phi(\mathbf{t}, h, w) = \phi(-\mathbf{t}, h, w)$ because, by definition, $\mathbf{t}$ and $-\mathbf{t}$ describe the same lead orientation]. The functional form $\boldsymbol{\sigma}(\dot{\varepsilon}, \mathbf{A}, \mathbf{R})$ derived satisfies continuum mechanics requirements of material frame indifference and dissipation.

Wilchinsky & Feltham (2004a, 2006a) derived equations governing the evolution of the state variables $\mathbf{A}$ and $\mathbf{R}$ of the form $\overset{\circ}{\mathbf{A}} = \Xi_A(\mathbf{A}, \dot{\varepsilon})$ and $\overset{\circ}{\mathbf{R}} = \Xi_R(\mathbf{R}, \dot{\varepsilon})$, where $^\circ$ denotes the Jaumann corotational time derivative. The mathematical derivations are too complex to repeat here, but the evolution equations account for lead formation and termination, narrowing (closing) and thickening under convergence, widening (opening) under divergence, rotation under shear, and the thermodynamic change of lead thickness through melting and freezing. To account for widening, narrowing, and extinction of leads, one must introduce an additional state variable,

$$\mathbf{C} = \langle w \mathbf{t} \otimes \mathbf{t} \rangle, \tag{35}$$

known as the width tensor, and a corresponding evolution equation, $\overset{\circ}{\mathbf{C}} = \Xi_C(\mathbf{C}, \dot{\varepsilon})$. The evolution equations for the state variables contain contractions of fourth-order

tensors with a strain rate that cannot be exactly represented in terms of the state variables. This constitutes a closure problem akin to that encountered in modeling velocity fluctuations in a turbulent Newtonian fluid, and it is addressed by approximating the relevant terms with forms shown to be accurate for low and high degrees of lead alignment.

Supplemental Appendix E presents an example of the evolution of state variables and sea ice stress for the case of pure shear deformation. Wilchinsky & Feltham (2006b) subsequently introduced a somewhat simpler anisotropic model of sea ice rheology based on the concept of leads defining diamond-shaped floe aggregates.

6. SUMMARY AND CONCLUDING REMARKS

The state of the cryosphere, and sea ice in particular, is undergoing significant changes, with rapid reductions in sea ice thickness (e.g., Rothrock et al. 1999) and extent (e.g., Stroeve et al. 2005) measured in the Arctic over the past few decades. These changes have led to increasing interest in the polar regions and acknowledgment of their intricate dynamics. Numerical calculations using sea ice models or climate models containing representations of sea ice demonstrate that the characteristics of the sea ice cover, such as its thickness and motion, depend at leading order on the representation of sea ice stress.

This review discusses the main theoretical contributions toward a continuum model of sea ice rheology suitable for climate prediction. The development of a definitive model of sea ice rheology, however, has been hampered by the lack of sufficient quantities of suitable data with which to test models of sea ice dynamics. Satellite passive microwave measurements have provided maps of ice extent and concentration (area fraction), but, until recently, measurements of sea ice thickness have been sparse and largely limited to observations of ice draft from submarines and moorings using upward-looking sonar, and drilling measurements at field sites. Additionally, uncertainties concerning the manner in which sea ice stress scales make it difficult to translate stress measurements at the field-site scale (approximately 0.1–1 km) or the laboratory scale (approximately 0.01–1 m) to the scale of a typical grid cell in a climate model, approximately 100 km (see **Supplemental Appendix C**). Thankfully, innovations in the remote sensing of sea ice afford cause for optimism: The exploitation of satellite altimetry has led to basinwide estimates of sea ice thickness in the Arctic (Laxon et al. 2003); improved feature-tracking algorithms have led to enhanced maps of sea ice motion; and high-resolution synthetic aperture radar imagery has led to unprecedented detail in maps of sea ice deformation (Kwok 2001). Confidence is now sufficiently great in remotely sensed data that it is beginning to be used to constrain the sea ice rheology used in models without arbitrary parameter tuning (e.g., Wilchinsky et al. 2006). Advances in computer technology have also made it possible to run regional models of the Arctic Ocean at very fine resolutions of approximately 10 km (Maslowski & Lipscomb 2003).

The combination of greater quantities of suitable data and understanding of the sources of error in the data, enhanced data processing, and more powerful computers has made it feasible to better characterize sea ice rheology in climate models. Observed

rapid change in the Arctic sea ice cover makes the study of sea ice rheology especially timely. This review discusses some aspects of the theoretical approaches taken to modeling anisotropy in the sea ice cover. Although these modeling approaches are at a relatively early stage, it seems reasonable to conclude that they may form the basis of the next generation of sea ice models. These models may be used for climate prediction or, perhaps, given the observed rapid reductions in Arctic sea ice, for the purposes of navigating trade routes.

DISCLOSURE STATEMENT

The author is not aware of any biases that might be perceived as affecting the objectivity of this review.

LITERATURE CITED

Coon MD, Knoke GS, Echert DC, Pritchard RS. 1998. The architecture of an anisotropic elastic-plastic sea ice mechanics constitutive law. *J. Geophys. Res.* 103:21915–25

Coon MD, Maykut GA, Pritchard RS, Rothrock DA, Thorndike AS. 1974. Modeling the pack ice as an elastic-plastic material. *AIDJEX Bull.* 24:1–105

Erlingsson B. 1988. Two-dimensional deformation patterns in sea ice. *J. Glaciol.* 34:301–8

Feltham DL. 2005. Granular flow in the marginal ice zone. *Philos. Trans. R. Soc. Lond. A* 363:1677–700

Gray JMNT, Morland LW. 1994. A two-dimensional model for the dynamics of sea ice. *Philos. Trans. R. Soc. Lond. A* 347:219–90

Gudkovich ZM, Nikiforov YeG. 1963. Stationary drift of a single floe. *Tr. Arkt. Anarkt.* 253

Hibler WD III. 1977. A viscous sea ice law as a stochastic average of plasticity. *J. Geophys. Res.* 82:3932–38

Hibler WD III. 1979. A dynamic thermodynamic sea ice model. *J. Phys. Oceanogr.* 9:815–46

Hibler WD III. 2001. Sea ice fracturing on the larger scale. *Eng. Fract. Mech.* 68:2013–43

Hibler WD III, Schulson EM. 2000. Anisotropic failure and flow of flawed sea ice. *J. Geophys. Res.* 105:17105–20

Hopkins MA. 1998. Four stages of pressure ridging. *J. Geophys. Res.* 103:21883–91

Hopkins MA, Frankenstein S, Thorndike AS. 2004. Formation of an aggregate scale in Arctic sea ice. *J. Geophys. Res.* 109:C01032

Hopkins MA, Tuhkuri J. 1999. Compression of floating ice fields. *J. Geophys. Res.* 104:15815–25

Hunke EC, Dukowicz JK. 1997. An elastic-viscous-plastic model for sea ice dynamics. *J. Phys. Oceanogr.* 27:1849–67

Hunter SC. 1983. *Mechanics of Continuous Media*. Chichester, UK: Ellis Horwood

Kwok R. 2001. Deformation of the Arctic Ocean sea ice cover between November 1996and April 1997: a qualitative survey. In *IUTAM Symposium on Scaling Laws in Ice Mechanics and Ice Dynamics*, ed. JP Dempsey, HH Shen, pp. 315–22. Dordrecht, Neth.: Kluwer Acad.

Laxon S, Peacock N, Smith D. 2003. High interannual variability of sea ice thickness in the Arctic region. *Nature* 425:947–50

Maslowski W, Lipscomb WH. 2003. High-resolution simulations of Arctic sea ice during 1979–1993. *Polar Res.* 22:67–74

Moritz RE, Ukita J. 2000. Geometry and the deformation of pack ice: I. a simple kinematic model. *Ann. Glaciol.* 31:313–22

Nansen F. 1902. The oceanography of the north polar basin: the Norwegian polar expedition 1893–1896. *Sci. Res.* 3:357–86

Overland JE, Pease CH. 1988. Modeling ice dynamics of coastal seas. *J. Geophys. Res.* 93:15619–37

Parmerter RR, Coon MD. 1973. Mechanical model of ridging in the Arctic sea ice cover. *AIDJEX Bull.* 19:59–112

Pritchard RS. 1975. An elastic-plastic constitutive law for sea ice. *J. Appl. Mech.* 42E:379–84

Pritchard RS. 1981. Mechanical behavior of pack ice. *Mech. Struct. Media*, *Proc. Symp. Struct. Media*, *Part A*, pp. 371–405. Amsterdam: Elsevier

Pritchard RS. 1988. Mathematical characteristics of sea ice dynamics models. *J. Geophys. Res.* 93:15609–18

Reed RS, Campbell WJ. 1960. Theory and observations of the drift of ice station Alpha. *ONR Final Rep.*, *Task No. NR 307–250. Tech. Rep.* Univ. Wash., Seattle

Rothrock DA. 1970. The pressure term in the constitutive law of an ice pack. *AIDJEX Bull.* 2:28–32

Rothrock DA. 1975. The energetics of the plastic deformation of pack ice by ridging. *J. Geophys. Res.* 80:4514–19

Rothrock DA, Yu Y, Maykut GA. 1999. Thinning of the Arctic sea-ice cover. *Geophys. Res. Lett.* 26:3469–72

Ruzin MI. 1959. The wind drift of ice in a heterogeneous pressure field. *Tr. Arkt. Antartkt. Inst.* 226:123–35

Schofield A, Wroth P. 1968. *Critical State Soil Mechanics*. New York: McGraw-Hill

Schreyer HL, Sulsky DL, Munday LB, Coon MD, Kwok R. 2006. Elastic-decohesive constitutive model for sea ice. *J. Geophys. Res.* 3:C11S26

Schulson EM. 2004. Compressive shear faults within Arctic ice: fracture on scales large and small. *J. Geophys. Res.* 109:C07016

Shen HH, Hibler WD III, Leppäranta M. 1987. The role of floe collisions in sea ice rheology. *J. Geophys. Res.* 92:7085–96

Solomon H. 1970. A study of ice dynamics relevant to AIDJEX. *AIDJEX Bull.* 2:33–50

Steele M, Zhang J, Rothrock D, Stern H. 1997. The force balance of sea ice in a numerical model of the Arctic Ocean. *J. Geophys. Res.* 102:21061–79

Stern HI, Rothrock DA, Kwok R. 1995. Open water production in Arctic sea ice: satellite measurements and model parameterisations. *J. Geophys. Res.* 100:20601–12

Stroeve JC, Serreze MC, Fetterer F, Arbetter T, Meier W, et al. 2005. Tracking the Arctic's shrinking ice cover: another extreme September minimum in 2004. *Geophys. Res. Lett.* 32:L04501

Thorndike AS, Rothrock DA, Maykut GA, Colony R. 1975. The thickness distribution of sea ice. *J. Geophys. Res.* 80:4501–13

Tremblay LB, Mysak LA. 1997. Modelling sea ice as a granular material, including the dilatancy effect. *J. Phys. Oceanogr.* 27:2342–60

Truesdell C, Noll W. 1965. *The Nonlinear Field Theories of Mechanics. Vol. 3*, *Encyclopedia of Physics*, ed. S Flügge. Berlin: Springer-Verlag

Ukita J, Moritz RE. 1995. Yield curves and flow rules of pack ice. *J. Geophys. Res.* 100:4545–57

Ukita J, Moritz RE. 2000. Geometry and the deformation of pack ice. II. Simulation with a random isotropic model and implication in sea-ice rheology. *Ann. Glaciol.* 31:323–26

Wilchinsky AV, Feltham DL. 2004a. A continuum anisotropic model of sea-ice dynamics. *Proc. R. Soc. Lond. A* 460:2105–40

Wilchinsky AV, Feltham DL. 2004b. Dependence of sea ice yield curve shape on ice thickness. *J. Phys. Oceanogr.* 34:2852–56

Wilchinsky AV, Feltham DL. 2006a. Anisotropic model for granulated sea ice dynamics. *J. Mech. Phys. Solids* 54:1147–85

Wilchinsky AV, Feltham DL. 2006b. Modelling the rheology of sea ice as a collection of diamond-shaped floes. *J. Non-Newton. Fluid Mech.* 138:22–32

Wilchinsky AV, Feltham DL, Miller P. 2006. A multi-layer sea ice model accounting for sliding friction. *J. Phys. Oceanogr.* 36:1719–38

Annual Review of
Fluid Mechanics

Volume 40, 2008

Contents

Indexes

Errata

An online log of corrections to *Annual Review of Fluid Mechanics* articles may be found at http://fluid.annualreviews.org/errata.shtml